Nucleation and Growth of Mineralized Bone Matrix on Silk-Hydroxyapatite Composite Scaffolds

Sarindr Bhumiratana[1], **Warren Grayson**[2], **Andrea Castaneda**[1], **Danielle Rockwood**[3], **Eun Seok Gil**[3], **David L. Kaplan**[3], and **Gordana Vunjak-Novakovic**[1],*

[1]Department of Biomedical Engineering, Columbia University, 622 W 168th Street, VC 12-234, New York, NY 10032

[2]Department of Biomedical Engineering, Johns Hopkins University, 400 N. Broadway, Smith Bldg. Rm 5023, Baltimore, MD 21231

[3]Department of Biomedical Engineering, Tufts Universty, 4 Colby St, Medford, MA 02155

Introduction

Bone repair procedures often require a replacement graft to restore the function of damaged or diseased tissue. These grafts are in most cases derived from tissues harvested from a second anatomic location of the same patient (autografts) or from other patients (allografts). Autografts have been considered the gold standard for bone repair. However, limited supplies of suitable bone grafts, donor site morbidity and difficulties in shaping explanted bone have posed significant problems. On the other hand, allografts have a risk of disease transmission [1]. These limitations provide incentives for finding alternative methods. Tissue engineered bone offers a promising alternative treatment for clinical use, as well as a controllable model system for studies of cell function, developmental biology and pathogenesis [2,3].

Successfully engineered bone grafts must be biocompatible and meet certain minimal mechanical requirements to be functional. The scaffold material provides many of the mechanical properties of the engineered graft. Organic- and polymer-based scaffolds are easily fabricated into different structures but often do not have the desired compressive modulus [4-7]. Alternatively, ceramic scaffolds are stiffer but are often fragile and have low porosity, resulting in loosening or fracture of implants in clinical applications [8]. Combining both types of materials to form composite scaffolds can enhance the mechanical and biochemical properties of scaffolds used for bone tissue engineering. In this study, silk protein and hydroxyapatite (HA) ceramic were chosen because of their biocompatibility and osteoconductivity, and ease and reproducibility of fabrication. Silk sponges have been used extensively in bone tissue engineering approaches with human mesenchymal stem cells (hMSCs) and shown to facilitate bone formation in vitro and in vivo [7,9-11]. Silk prepared with organic solvent (hexafluoroisopropanol: HFIP) and salt leeching allows the fabrication of biocompatible scaffolds with high silk content, high porosity, and good inter-pore

* To Whom Correspondence Should Be Addressed: Dr. Gordana Vunjak-Novakovic, Columbia University, Department of Biomedical Engineering, 622 West 168th Street, VC12-234, New York NY, 10032, gv2131@columbia.edu.

connectivity [7,9,12]. HA also has excellent biocompatibility and bioactivity, is osteo-inductive and is slowly replaced by host bone after implantation [13-16]. We hypothesized that embedding HA micro-particles within the walls of silk sponges would improve scaffold stiffness and enhance hMSC differentiation resulting in the development of tissue engineered bone grafts with higher mineral content and improved compressive stiffness. We therefore examined the effects of scaffold properties on the structural and mechanical outcomes of engineered bone grafts by incorporating various amounts of HA mineral in porous silk scaffolds.

Bone-like constructs have been prepared *in vitro* by culturing hMSCs seeded into biomaterial scaffolds. HMSCs offer several advantages: they can be obtained autologously, expanded *in vitro* to provide sufficient cell numbers, differentiated into osteoblasts [17-20] and have shown promising results in clinical models [21]. In this study, silk-HA scaffolds were seeded with hMSCs and cultured in perfusion bioreactors, which improve cell distribution and bone formation inside the scaffolds [22-24]. Perfusion provides adequate nutrient and oxygen supplies as well as cell stimulation through fluid shear stress, which enhances hMSCs osteogenic differentiation [24-27]. Constructs were cultured for up to 10 weeks before being harvested and analyzed for bone tissue formation.

Materials and Methods

Scaffold Fabrication

All reagents were purchased from Sigma Aldrich (St. Louis, MO) unless otherwise specified. Silk fibroin was extracted from *Bombyx mori* cocoons utilizing our previously developed methods [12]. Briefly, the sericin was removed by boiling the cocoons in a 0.02 M Na_2CO_3 solution for 30 minutes. The resulting fibers were then dissolved in 9.3 M LiBr for 4 hours at 60°C and then subsequently dialyzed against ultrapure water for 48 hours to remove residual LiBr. The aqueous silk solutions were lyophilized and redissolved in HFIP to yield a solution of 16 w/v%. The method for fabricating HA-incorporated silk sponges is shown in Fig.1A. Reinforcement of the scaffolds was achieved by mixing HA into the NaCl particles and then pouring the silk solution over the mixture. Scaffolds were prepared with pore sizes ranging between 500 and 600 mm using granular NaCl as a porogen. Once the scaffolds solidified, they were treated with methanol for 1-2 days to induce β-sheet formation and then the salt was subsequently extracted by immersion in fresh water for 48 hrs. Scaffolds were cut and cored into cylinders of 4 mm in diameter by 4 mm thick and were sterilized in 70% ethanol overnight and incubated in culture medium over night before seeding.

Four groups of scaffolds with different content of HA-silk composition were fabricated with mixtures of Silk:HA:Salt ratios by weight of 1:0:20, 1:0.5:20, 1:1:20, and 1:1.5:20. The volume fractions of silk and HA in the porous scaffold were calculated using the amount of the materials added and their densities which are 1.4 g/ml and 3.16 g/ml, respectively. As a result, the designated group names were based on approximated HA volume fraction in the scaffolds which were 0%, 1.6%, 3.1%, and 4.6% HA, respectively.

Scanning electron microscopy

SEM was performed to determine pore structure and surface topography on two scaffolds of each group. In brief, scaffolds were washed in PBS and then fixed in 2% glutaraldehyde in PBS overnight. Constructs were washed in alcohol gradient up to 70% and then freeze-dried overnight in a lyophilizer. Dried samples were coated with gold and imaged at 200× and 1000× in an SEM (JEOL, Japan).

Human Mesenchymal Stem Cell Cultivation and Seeding

Fresh bone marrow aspirates were obtained from Cambrex Life Sciences (East Rutherford, NJ), isolated and characterized as previously described [23]. Cells were expanded in high-glucose DMEM supplemented with 10% FBS, 1% pen-strep, and 0.1 ng/mL bFGF. The hMSCs were cultured up to the third passage and then used for seeding the scaffolds. The seeding process was previously described [7,28]. In brief, scaffolds were seeded at the concentration of 30×10^6 cells per 1 ml of scaffold. A 40-μl aliquot of cell suspension was pipetted onto blot-dried scaffolds and allowed to percolate through. The scaffolds were flipped 180° every 20 minutes and 10 μl of media was added to prevent the cells from drying out. Constructs were cultured with osteogenic medium (low-glucose DMEM supplemented with 10% FBS, 10 nM dexamethasone, 10 mM sodium-β-glycerophosphate, and 0.05 mM ascorbic acid-2-phosphate) for 3 days before harvested for Day 0 sample and insertion into the bioreactor.

Bioreactor Cultivation

A perfusion bioreactor developed in our laboratory and described and used previously [22,28] was employed in this study. In brief, 6 scaffolds were placed in each bioreactor and medium flow rate was set to provide the superficial velocity of medium through the scaffolds at 400 μm/s. Half of the medium volume was replaced twice a week and scaffolds were harvested for analysis at week 5 and 10 (Fig.1B). The studies were conducted twice 6 month apart with different batches of scaffolds to ensure reproducible results. Since the results of the two studies were similar, they were pooled together. Two additional experimental groups (unseeded 0% HA and 4.6% HA) were performed in the repeat experiment (Fig.1B).

Cell Viability

After harvest at day 0 and week 10, two half scaffolds per group were washed in PBS and stained with 1 mM calcein and 4 mM ethidium in PBS for 30 min. The images were taken with a confocal microscope (Leica, Germany; 20 slices at 10 μm thick).

Biochemical Assay

Constructs were cut in half in the longitudinal direction, washed in PBS and the wet weights were determined. For DNA analysis, the samples (n=8) were stored at -20°C in 1 ml of digestion buffer (10 mM Tris, 1mM EDTA and 0.1% Triton X-100) with 0.1 mg/ml of proteinase K in micro-centrifuge tubes. Samples were then thawed and maintained in this solution overnight at 56°C to extract the DNA. The DNA content was determined using a Picogreen assay (Molecular Probes, OR). For calcium content analysis, the samples (n=4) were quickly frozen in liquid nitrogen and stored at -20°C. Calcium was extracted in 500 μl of 5% TCA solution using a bead beater and analyzed with a Calcium (CPC) Liquicolor® kit (Stanbio Laboratory, USA).

Mechanical Testing

The equilibrium compressive Young's modulus (n=8 per group) was determined at day 0, week 5, and week 10 under unconfined compression in wet conditions using a modification of an established protocol [29]. An initial tare load of 0.2 N was applied and was followed by a stress-relaxation step where specimens were compressed at a ramp velocity of 1% per second up to 10% strain and maintained at the position for 1800 s. The Young's modulus was obtained from the equilibrium forces measured at 10% strain. Mechanical properties of decellularized trabecular bovine bones were also measured with the same method.

Micro Computerized Tomography

μCT imaging was performed using a modification of a previously used protocol [30] with the following settings: voltage 55kV, current 0.109 mA, slice thickness 21 μm, and inter-slice spacing 22 μm. Scaffolds were scanned prior to seeding and after cultivation. Immediately after harvesting, full constructs (n=6 per group) were aligned and stabilized along their axial direction in PBS inside microcentrifuge tubes. The tubes were placed in the specimen holder of a vivaCT 40 system (SCANCO Medical AG, Basserdorf, Switzerland). Constructs were scanned at 21 μm isotropic resolution. The bone volume was obtained using a global thresholding technique with threshold at 220. The structural parameters, which are bone volume (BV), bone volume fraction (BVF), connectivity density (Conn.D), trabecular number (Tb.N), trabecular thickness (Tb.Th), and trabecular spacing (Tb.Sp) were determined with the structural reconstruction. Decellularized trabecular bovine bones were also scanned in parallel to compare with the cultured constructs.

Histology and Immunohistochemistry

Constructs were washed in PBS, fixed in 10% formalin, embedded in paraffin, sectioned into 4 μm slices and stained with haematoxylin and eosin (H&E), and Von Kossa. Immunohistochemistry staining for collagen type I, bone sialoprotein (BSP), and osteopontin was also conducted as previously described [28].

Statistical Analysis

Multiway Analysis of Variance (ANOVA) to analyze groups at the same time point and within group at different time points was carried out followed by Tukey's *post hoc* analysis using STATISTICA software, with $p < 0.05$ being considered as significant.

Results

Scaffold Fabrication

The inter-pore connectivity of the scaffolds was maintained with the incorporation of HA into the silk sponges, while minimally reducing the porosity as seen in low magnification SEM images (Fig. 2). The pore size of the scaffolds in all groups ranged between 400-600 μm, which is equivalent to the size of the salt particles that were used in the process. High magnification SEM images showed an increase in scaffold surface roughness qualitatively as more HA was added, but with less distinct differences between 3.1% and 4.6% groups (Fig.2). The incorporated HA was trapped within the silk structure and an increase in wall thickness was observed. By converting material mass introduced into the scaffold into volume, the total material volume fraction within the 0%, 1.6%, 3.1%, and 4.6% HA groups were 7.18, 8.66, 10.04, and 11.40%, respectively; thus, a decrease in void volume was observed as more HA was incorporated. In addition, incorporation of HA gradually increased scaffold equilibrium compressive Young's modulus measured in the hydrated state, from 120.8±48.7 kPa in 0% HA group to 251.1±116.9 kPa in 4.6% HA group (Fig. 4A).

Cell Viability and DNA Content

After 5 and 10 weeks of culture, the DNA content significantly increased from Day 0 in all groups and as much as 4 fold in the 4.6% HA (Fig.3A). Although the average DNA content of the 0% HA was significantly higher than in the 3.1% and 4.6% HA groups at Day 0, the DNA content was not significantly different after 5 and 10 weeks of culture. Live/Dead assay showed good cell viability after seeding and after 10 weeks of culture with an increase in cell content over the culture period (Fig. 3B).

Mineral Content and Micro-Structure

The structure of the tissue engineered bone developed over 5 and 10 weeks of culture (Fig. 4). In the 0% HA group, the tissue engineered bone had no detectable mineral with µCT and, while over 10 weeks, the mineral deposited developed into spherical-like structures (Fig. 4). Constructs from the 1.6% HA group developed into trabecular-like structures over the culture period with some aggregates of spherical-like structures (Fig. 4). In contrast, constructs in the 3.1% and 4.6% HA groups developed trabecular-like architectures with high structural connectivity (Fig. 4).

Quantification of morphological parameters confirmed development of trabecular-like structures in 3.1% and 4.6% HA groups (Fig.5). BV, BVF, Conn.D, Tb.N, Tb.Th, and Tb.Sp approached the values of native bovine trabecular bone (dash lines) determined in our laboratory with the same scanning method. BV, BVF, and Conn.D significantly increased and more than doubled over 10 weeks of culture in the groups with mineral. The BVF (Fig. 3D) of 3.1% and 4.6% HA on average were 0.029 ± 0.028 and 0.068 ± 0.038 at day 0 and reached 0.097 ± 0.021 and 0.126 ± 0.019 at 5 weeks and 0.142 ± 0.062 and 0.156 ± 0.033 at 10 weeks, respectively. The Conn.D (Fig. 5E) of 3.1% and 4.6% HA increased significantly from 0.78 ± 1.72 and 2.34 ± 2.57 $1/mm^3$ to 4.18 ± 1.85 and 8.76 ± 2.40 $1/mm^3$ at week 5 and to 9.24 ± 8.53 and 12.83 ± 5.43 $1/mm^3$ at week 10, respectively. Tb.N and Tb.Th increased over time while the Tb.Sp decreased (Fig. 5F-H) in all groups except 0% HA in which Tb.Sp at day 0 could not be determined. When unseeded 0% HA and 4.6% HA were cultured for 5 weeks, all parameters remained the same as the day 0 value, indicating that changes in mineralization were cell-based (data not shown).

Mechanical Properties

The equilibrium Young's modulus gradually increased over time in all groups (Fig. 5A). The moduli of scaffolds containing 0%, 1.6%, 3.1%, and 4.6% HA were 121 ± 49, 140 ± 70, 201 ± 90, and 251 ± 117 kPa, respectively, at Day 0. By 5 weeks, the moduli of scaffolds containing 0%, 1.6%, 3.1%, and 4.6% HA reached, 340 ± 99, 594 ± 234, 865 ± 347, and 1005 ± 381 kPa, respectively. The modulus of the 3.1% and 4.6% HA were significantly higher than the modulus of the 0% HA. Equilibrium Young's moduli of unseeded 0% and 4.6% HA were not significantly different from day 0. By 10 weeks, the moduli of scaffolds containing 0%, 1.6%, 3.1%, and 4.6% HA reached on average 0.532 ± 0.180, 0.869 ± 297, 1.600 ± 0.577, and 1.670 ± 0.528 MPa, respectively. The moduli of scaffolds containing 3.1% and 4.6% HA were significantly higher than the moduli of both 0% and 1.6% HA. The equilibrium Young's moduli of decellularized bovine trabecular bone determined in our laboratory with the same method ranged between 5-40 MPa. The equilibrium Young's moduli of unseeded 0% HA and 4.6% HA remained unchanged from the Day 0 value.

Calcium Content

The calcium content of scaffolds increased over time but the increases were not statistically significant within each group (Fig. 5B). At Day 0, the calcium content of scaffolds containing 0%, 1.6%, 3.1%, and 4.6% HA were 0 ± 0, 1.18 ± 0.85, 2.21 ± 1.32, and 3.47 ± 1.00 mg per scaffold, respectively. Over 10 weeks, the average calcium content increased by 0.24, 0.40, 0.97, and 0.90 mg per scaffold for scaffolds containing 0%, 1.6%, 3.1%, and 4.6% HA, respectively. Both unseeded 0% and 4.6% HA did not show an increase in average calcium content (data not shown).

Histology and Immunohistochemistry

H&E (Fig. 6A) shows increased cell content in pore spaces within the first 5 weeks of culture in accordance with DNA quantification. As seen by von Kossa staining, there was an

increase in calcium content within scaffold structure as more HA was incorporated and this resulted in thicker walls, similar to the structures seen by SEM. Over 5 and 10 weeks, the 0% and 1.6% HA exhibited a deposition of mineral in the scaffold pores while such evidence was not observed in the 3.1% and 4.6% HA. The mineral inside the pore space of 0% HA aggregated forming granular structures. Collagen type I (Fig. 6C), BSP (Fig. 6D), and OCN (data not shown) immunohistochemistry staining indicated an increase in bone matrix deposition over time in all group. The staining of the proteins was most intense in 3.1% and 4.6% HA at 10 weeks of culture.

Discussion

Silk has shown significant promise as a biomaterial for bone tissue engineering scaffolds [4,31,32]. However, silk by itself is not osteogenic, and the mechanical properties of silk scaffolds are considerably lower than those of native bone (Young's moduli ~ 100 kPa vs. ~ 10 MPa for bone). In the present study, we investigated the potential of HA micro-particles to improve the osteogenic and mechanical properties of silk scaffolds, and enhance the *in vitro* formation of bone-like tissues by hMSCs without the use of osteogenic growth factors such as BMPs.

We successfully fabricated biocompatible HA-embedded silk scaffolds while maintaining pore size and interconnectivity (Fig. 2). The incorporation of HA altered scaffold surface chemistry, increased surface roughness (Fig. 2) and increased the stiffness of unseeded scaffolds (Fig. 5A) We confirmed that HA was osteoinductive as the mineral deposition increased in a dose-dependent response to the initial amount of HA as demonstrated with μCT imaging (Fig. 4). The major contribution of the HA was to guide the deposition of the newly formed bone mineral to provide significantly higher construct mechanical stiffness at the end of cultivation. Previous findings suggest that the microarchitecture (topography, orientation and connection of trabeculae), in addition to bone volume fraction, are important in governing the mechanical properties of trabecular bone [30,33].

The compressive (Young) modulus of engineered bone constructs increased as much as 8-fold for HA scaffolds when compared to silk alone (Fig. 5A), approaching that of the decellularized bovine trabecular bone measured via the same testing method. We found that 3.1% HA mineral provided sufficient bioactivity to direct hMSCs to form a trabecular-like mineral structure. Thus, the significant increase in the strength of engineered bone constructs in the present study was likely due to the combination effect of the changes in the amount of mineral (as seen from increased bone volume fractions, Fig. 5D) and the improved structure (as seen from increased bone interconnectivity, Fig. 5E). In contrast, an increase in the trabecular thickness of pure silk scaffolds with no concomitant change in connectivity confirmed an increase in size of spherical mineral deposits, which did not significantly improve the mechanical properties [7,10,11,34]. In all cases, histological von Kossa staining confirmed the μCT data.

Calcium production by the differentiated hMSCs correlated with the amount of embedded HA in a dose dependent manner up to 3.1% HA and remained constant thereafter, which was consistent with prior reports [35-37]. With the same number of cells among the study groups, the amount of calcium deposition in the 3.1% and 4.6% HA groups was in creased by almost 4-fold as compared to the 0% HA group. However, due to the high initial values of calcium in the HA scaffolds compared to the amount of calcium produced by the cells, the increase in calcium content was steady but not statistically significant over time. Previous studies reported calcium production by hMSCs ranging from 0.25 to 8 μg/ng DNA after 5 weeks of culture in osteogenic medium supplemented with BMP-2 [7,34,38].

Calcium production in the present study was 0.11 μg/ng DNA over 10 weeks, a lower amount as no BMP-2 was supplemented to the cultures.

An interesting observation was that the increase in bone volume (Fig. 5C) analyzed by μCT was substantially higher than the increase in calcium content (Fig. 5B). It appears that since μCT employed in this study has a resolution of 21 μm and the largest HA particles observed by SEM imaging was approximately 20 μm, not mineral was detected by μCT. Therefore, the change in bone volume measured by μCT included both the initially undetected HA microparticles that grew larger and the new mineral produced by cells. These HA microparticles therefore played a role of nucleation sites that facilitated the formation of a highly connected mineral structure. In addition to the production of mineral, the production of bone matrix proteins was also dependent on HA concentration, as seen with collagen type I and BSP (Fig. 6C,D), and consistent with the effect of HA mineral on gene expression previously reported [39,40]. The unseeded scaffolds of the 0% and 4.6% HA groups did not demonstrate changes in mineral structure, calcium content, bone matrix production or mechanical strength, indicating that these changes were cell-mediated.

It is also possible that the enhanced outcomes in the HA scaffolds may be explained in part due to the changes in the initial stiffness and surface roughness, both of which may influence cellular responses. However, initial scaffold stiffness was not significantly altered among the groups and other forms of modifying silk scaffolds have provided considerably higher initial compressive moduli but did not elicit such significant cell-mediated improvements [9]. Therefore, it is unlikely that the surface roughness of the scaffolds was the main reason for large improvement in mechanical properties, as a previous attempt to mineralize silk scaffolds through surface coating with HA did not elicit the same response [40]. By incorporating HA into the walls of the silk scaffolds, we provided the hMSCs with a more osteoinductive surface, but more crucially, the data suggests that the HA microparticles served as nucleation sites that directed mineral deposition, leading to an enhanced trabecular structure, increased connectivity and superior mechanical properties of the resulting tissue grafts. This is shown schematically in Fig. 7. Such a mechanism suggests that the spatial proximity of HA microparticles to each other is an important parameter and may also explain why the increase from 3.1% to 4.6% HA did not elicit a pronounced difference in the final outcome, as a certain threshold distance between neighboring particles had been attained.

Conclusions

The effect of incorporating the HA mineral into porous silk scaffolds was investigated for tissue engineered bone formation with hMSCs. The HA mineral enhanced hMSCs osteogenic differentiation and provided a platform for bone-like structure formation when adequate HA content was incorporated. The HA mineral provided a platform for the formation of engineered bone by hMSCs, both through the osteoconductivity of the material and by providing nucleation sites for the newly produced mineral.

Acknowledgments

References

1. Khan Y, Yaszemski MJ, Mikos AG, Laurencin CT. Tissue engineering of bone: material and matrix considerations. J Bone Joint Surg Am 2008;90 1:36–42. [PubMed: 18292355]

2. Griffith LG, Naughton G. Tissue engineering--current challenges and expanding opportunities. Science 2002;295(5557):1009–14. [PubMed: 11834815]

3. Langer R, Vacanti JP. Tissue engineering. Science 1993;260(5110):920–6. [PubMed: 8493529]

4. Kim HJ, Kim UJ, Vunjak-Novakovic G, Min BH, Kaplan DL. Influence of macroporous protein scaffolds on bone tissue engineering from bone marrow stem cells. Biomaterials 2005;26(21):4442–52. [PubMed: 15701373]

5. Martin I, Shastri VP, Padera RF, Yang J, Mackay AJ, Langer R, et al. Selective differentiation of mammalian bone marrow stromal cells cultured on three-dimensional polymer foams. J Biomed Mater Res 2001;55(2):229–35. [PubMed: 11255174]

6. Ishaug SL, Crane GM, Miller MJ, Yasko AW, Yaszemski MJ, Mikos AG. Bone formation by three-dimensional stromal osteoblast culture in biodegradable polymer scaffolds. J Biomed Mater Res 1997;36(1):17–28. [PubMed: 9212385]

7. Marolt D, Augst A, Freed LE, Vepari C, Fajardo R, Patel N, et al. Bone and cartilage tissue constructs grown using human bone marrow stromal cells, silk scaffolds and rotating bioreactors. Biomaterials 2006;27(36):6138–49. [PubMed: 16895736]

8. Waite PD, Morawetz RB, Zeiger HE, Pincock JL. Reconstruction of cranial defects with porous hydroxylapatite blocks. Neurosurgery 1989;25(2):214–7. [PubMed: 2549443]

9. Rockwood DN, Gil ES, Park SH, Kluge JA, Grayson W, Bhumiratana S, et al. Ingrowth of human mesenchymal stem cells into porous silk particle reinforced silk composite scaffolds: An in vitro study. Acta Biomater 2011;7(1):144–51. [PubMed: 20656075]

10. Augst A, Marolt D, Freed LE, Vepari C, Meinel L, Farley M, et al. Effects of chondrogenic and osteogenic regulatory factors on composite constructs grown using human mesenchymal stem cells, silk scaffolds and bioreactors. J R Soc Interface 2008;5(25):929–39. [PubMed: 18230586]

11. Meinel L, Karageorgiou V, Hofmann S, Fajardo R, Snyder B, Li C, et al. Engineering bone-like tissue in vitro using human bone marrow stem cells and silk scaffolds. J Biomed Mater Res A 2004;71(1):25–34. [PubMed: 15316936]

12. Nazarov R, Jin HJ, Kaplan DL. Porous 3-D scaffolds from regenerated silk fibroin. Biomacromolecules 2004;5(3):718–26. [PubMed: 15132652]

13. Na K, Kim SW, Sun BK, Woo DG, Yang HN, Chung HM, et al. Osteogenic differentiation of rabbit mesenchymal stem cells in thermo-reversible hydrogel constructs containing hydroxyapatite and bone morphogenic protein-2 (BMP-2). Biomaterials 2007;28(16):2631–7. [PubMed: 17331575]

14. Bucholz RW, Carlton A, Holmes RE. Hydroxyapatite and tricalcium phosphate bone graft substitutes. Orthop Clin North Am 1987;18(2):323–34. [PubMed: 3561978]

15. Radin SR, Ducheyne P. Effect of bioactive ceramic composition and structure on in vitro behavior. III. Porous versus dense ceramics. J Biomed Mater Res 1994;28(11):1303–9. [PubMed: 7829560]

16. Redey SA, Razzouk S, Rey C, Bernache-Assollant D, Leroy G, Nardin M, et al. Osteoclast adhesion and activity on synthetic hydroxyapatite, carbonated hydroxyapatite, and natural calcium carbonate: relationship to surface energies. J Biomed Mater Res 1999;45(2):140–7. [PubMed: 10397968]

17. Friedenstein AJ, Chailakhyan RK, Gerasimov UV. Bone marrow osteogenic stem cells: in vitro cultivation and transplantation in diffusion chambers. Cell Tissue Kinet 1987;20(3):263–72. [PubMed: 3690622]

18. Pittenger MF, Mackay AM, Beck SC, Jaiswal RK, Douglas R, Mosca JD, et al. Multilineage potential of adult human mesenchymal stem cells. Science 1999;284(5411):143–7. [PubMed: 10102814]

19. Mauney JR, Kaplan DL, Volloch V. Matrix-mediated retention of osteogenic differentiation potential by human adult bone marrow stromal cells during ex vivo expansion. Biomaterials 2004;25(16):3233–43. [PubMed: 14980418]

20. Derubeis AR, Cancedda R. Bone marrow stromal cells (BMSCs) in bone engineering: limitations and recent advances. Ann Biomed Eng 2004;32(1):160–5. [PubMed: 14964731]

21. Cancedda R, Bianchi G, Derubeis A, Quarto R. Cell therapy for bone disease: a review of current status. Stem Cells 2003;21(5):610–9. [PubMed: 12968115]

22. Grayson WL, Bhumiratana S, Grace Chao PH, Hung CT, Vunjak-Novakovic G. Spatial regulation of human mesenchymal stem cell differentiation in engineered osteochondral constructs: effects of

pre-differentiation, soluble factors and medium perfusion. Osteoarthritis Cartilage 2010;18(5): 714–23. [PubMed: 20175974]

23. Grayson WL, Frohlich M, Yeager K, Bhumiratana S, Chan ME, Cannizzaro C, et al. Engineering anatomically shaped human bone grafts. Proc Natl Acad Sci U S A 2010;107(8):3299–304. [PubMed: 19820164]

24. Bancroft GN, Sikavitsas VI, van den Dolder J, Sheffield TL, Ambrose CG, Jansen JA, et al. Fluid flow increases mineralized matrix deposition in 3D perfusion culture of marrow stromal osteoblasts in a dose-dependent manner. Proc Natl Acad Sci U S A 2002;99(20):12600–5. [PubMed: 12242339]

25. Porter B, Zauel R, Stockman H, Guldberg R, Fyhrie D. 3-D computational modeling of media flow through scaffolds in a perfusion bioreactor. J Biomech 2005;38(3):543–9. [PubMed: 15652553]

26. Datta N, Pham QP, Sharma U, Sikavitsas VI, Jansen JA, Mikos AG. In vitro generated extracellular matrix and fluid shear stress synergistically enhance 3D osteoblastic differentiation. Proc Natl Acad Sci U S A 2006;103(8):2488–93. [PubMed: 16477044]

27. Li YJ, Batra NN, You L, Meier SC, Coe IA, Yellowley CE, et al. Oscillatory fluid flow affects human marrow stromal cell proliferation and differentiation. J Orthop Res 2004;22(6):1283–9. [PubMed: 15475210]

28. Grayson WL, Bhumiratana S, Cannizzaro C, Chao PH, Lennon DP, Caplan AI, et al. Effects of initial seeding density and fluid perfusion rate on formation of tissue-engineered bone. Tissue Eng Part A 2008;14(11):1809–20. [PubMed: 18620487]

29. Mauck RL, Soltz MA, Wang CC, Wong DD, Chao PH, Valhmu WB, et al. Functional tissue engineering of articular cartilage through dynamic loading of chondrocyte-seeded agarose gels. J Biomech Eng 2000;122(3):252–60. [PubMed: 10923293]

30. Liu XS, Sajda P, Saha PK, Wehrli FW, Guo XE. Quantification of the roles of trabecular microarchitecture and trabecular type in determining the elastic modulus of human trabecular bone. J Bone Miner Res 2006;21(10):1608–17. [PubMed: 16995816]

31. Hofmann S, Hagenmuller H, Koch AM, Muller R, Vunjak-Novakovic G, Kaplan DL, et al. Control of in vitro tissue-engineered bone-like structures using human mesenchymal stem cells and porous silk scaffolds. Biomaterials 2007;28(6):1152–62. [PubMed: 17092555]

32. Kim HJ, Kim UJ, Leisk GG, Bayan C, Georgakoudi I, Kaplan DL. Bone regeneration on macroporous aqueous-derived silk 3-D scaffolds. Macromol Biosci 2007;7(5):643–55. [PubMed: 17477447]

33. Jensen KS, Mosekilde L. A model of vertebral trabecular bone architecture and its mechanical properties. Bone 1990;11(6):417–23. [PubMed: 2078435]

34. Meinel L, Karageorgiou V, Fajardo R, Snyder B, Shinde-Patil V, Zichner L, et al. Bone tissue engineering using human mesenchymal stem cells: effects of scaffold material and medium flow. Ann Biomed Eng 2004;32(1):112–22. [PubMed: 14964727]

35. Okumura M, Ohgushi H, Dohi Y, Katuda T, Tamai S, Koerten HK, et al. Osteoblastic phenotype expression on the surface of hydroxyapatite ceramics. J Biomed Mater Res 1997;37(1):122–9. [PubMed: 9335357]

36. Cong Z, Jianxin W, Huaizhi F, Bing L, Xingdong Z. Repairing segmental bone defects with living porous ceramic cylinders: an experimental study in dog femora. J Biomed Mater Res 2001;55(1): 28–32. [PubMed: 11426394]

37. Norman ME, Elgendy HM, Shors EC, el-Amin SF, Laurencin CT. An in-vitro evaluation of coralline porous hydroxyapatite as a scaffold for osteoblast growth. Clin Mater 1994;17(2):85–91. [PubMed: 10150211]

38. Li C, Vepari C, Jin HJ, Kim HJ, Kaplan DL. Electrospun silk-BMP-2 scaffolds for bone tissue engineering. Biomaterials 2006;27(16):3115–24. [PubMed: 16458961]

39. Ma PX, Zhang R, Xiao G, Franceschi R. Engineering new bone tissue in vitro on highly porous poly(alpha-hydroxyl acids)/hydroxyapatite composite scaffolds. J Biomed Mater Res 2001;54(2): 284–93. [PubMed: 11093189]

40. Kim HJ, Kim UJ, Kim HS, Li C, Wada M, Leisk GG, et al. Bone tissue engineering with premineralized silk scaffolds. Bone 2008;42(6):1226–34. [PubMed: 18387349]
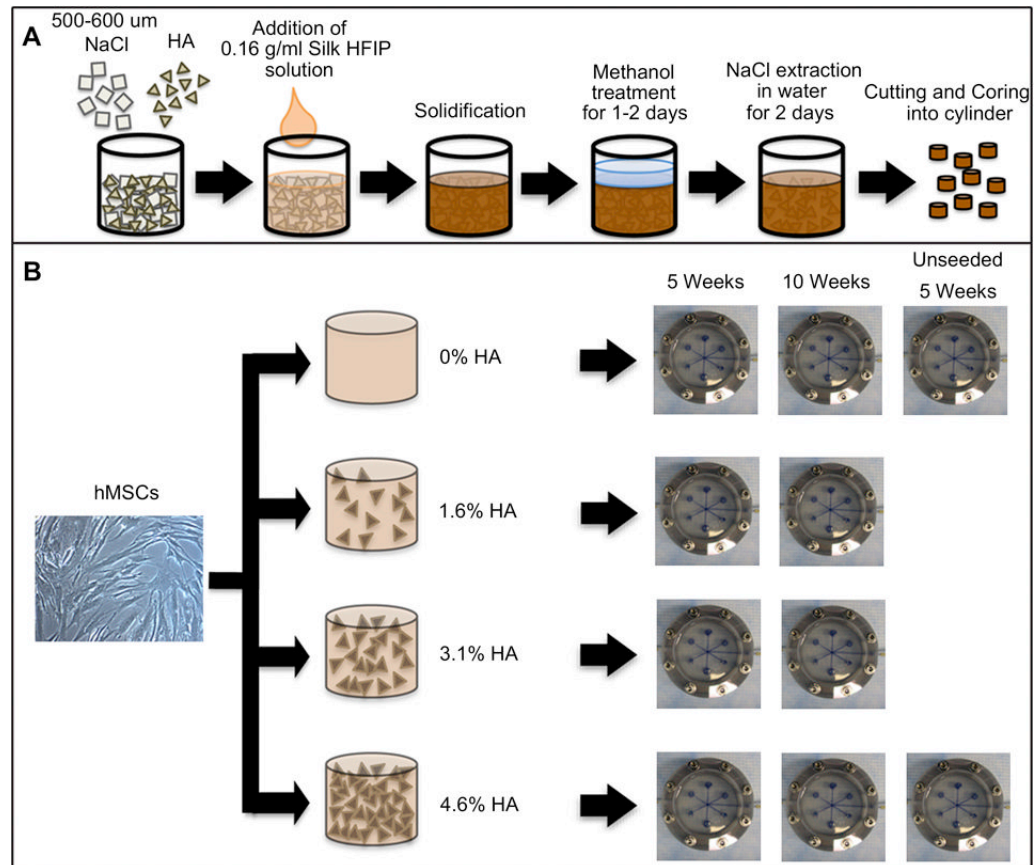
Figure 1.
(A) Silk-HA composite scaffold fabrication process. (B) Experimental design to study the effects of embedded HA content in silk sponge in formation of tissue engineered bone constructs. Four types of scaffolds (0% HA, 1.6% HA, 3.1% HA, and 4.6% HA) were seeded with hMSCs and cultured in osteogenic media under perfusion bioreactor for 5 and 10 weeks. Unseeded 0% HA and 4.6% HA were also cultured for 5 weeks.
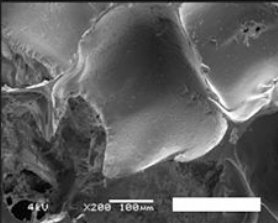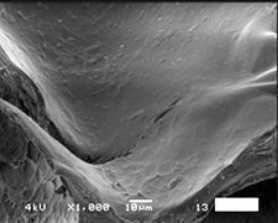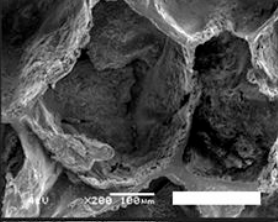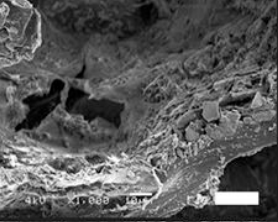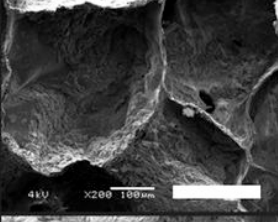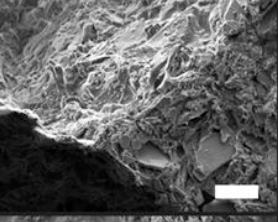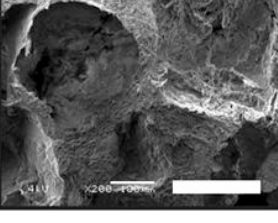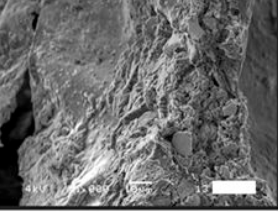
Group	Silk Content (%v)	Mineral Content (%v)	SEM Image 200x	SEM Image 1000x
0% HA	7.18	0		
1.6% HA	7.06	1.57		
3.1% HA	6.96	3.08		
4.6% HA	6.85	4.55		

Figure 2.
Calculated volume fraction of silk and HA mineral and SEM images of 0% HA, 1.6% HA, 3.1% HA, and 4.6% HA scaffolds. 200× SEM image showed porous scaffold with inter-pore connectivity (bar: 200 μm). 1000× SEM image illustrated the different in surface topography of the scaffolds (bar: 20 μm).
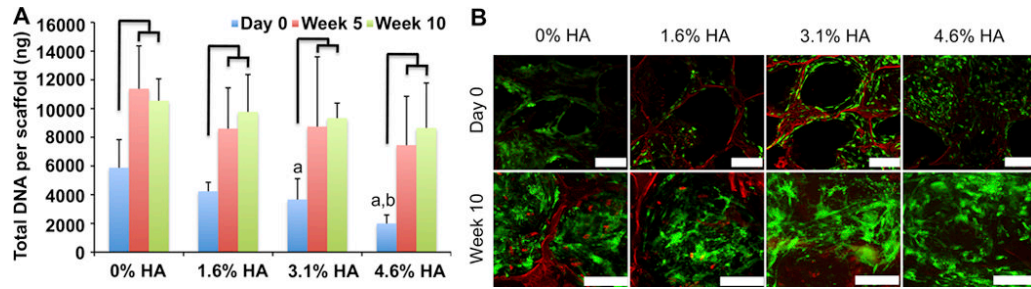
Figure 3.
(A) DNA content before and after cultivation in perfusion bioreactor for 5 and 10 weeks. (Line represents a statistically significant difference between time point of the same scaffold group; [a, b] represent statistically significant differences from 0% HA and 1.6% HA, respectively, at the same time point). (B) Live/Dead image of cells inside the scaffolds before and after cultivation for 10 weeks. (scale bar: 200 μm)
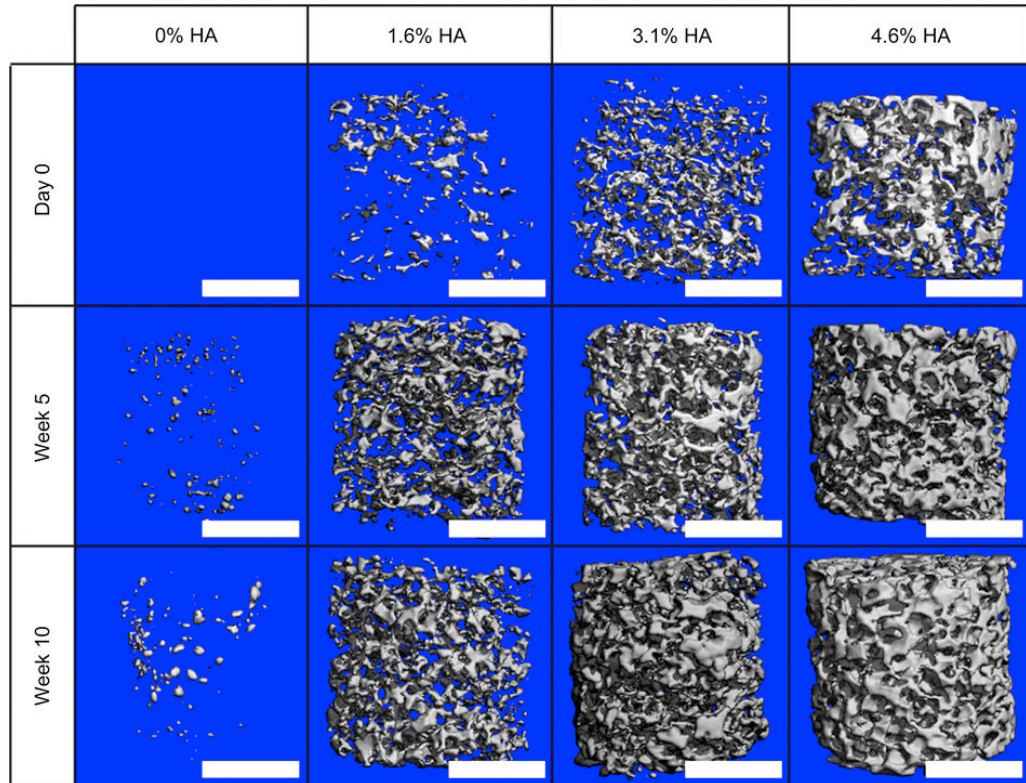
Figure 4.
Reconstructed 3D µCT images of the tissue engineered bone construct before and after cultivation for 5 and 10 weeks of all groups (scale bar: 2mm)
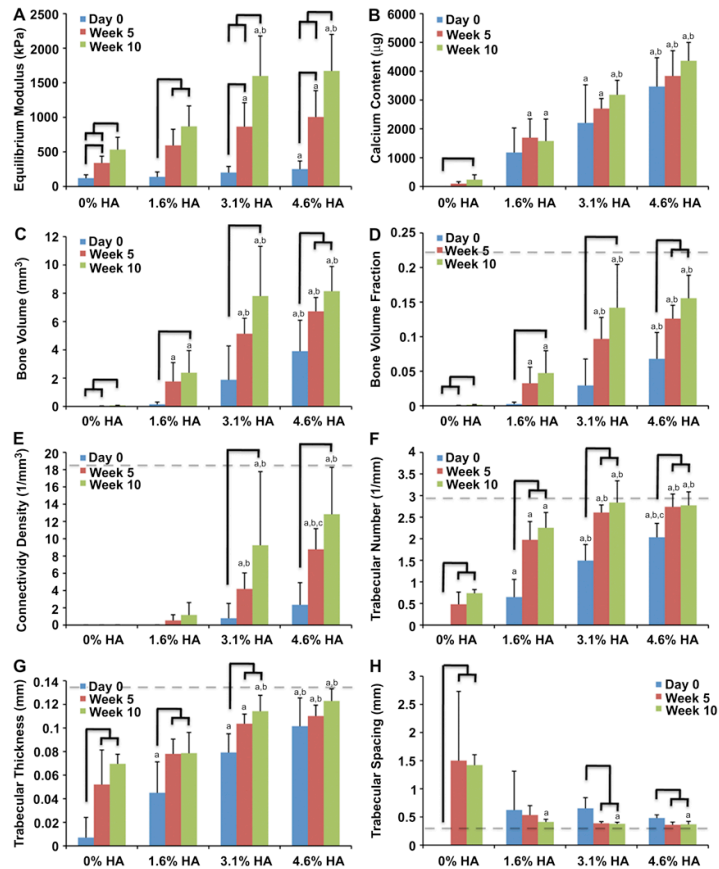
Figure 5.
Development of tissue engineered bone constructs over 5 and 10 weeks of cultivation: (A) Equilibrium Young's Modulus, (B) calcium content, and bone structural parameters determined by µCT analysis; (C) BV, (D) BVF, (E) Conn.D, (F) Tb.N, (G) Tb.Th, and (H) Tb.Sp. (Dash line indicates average value of decellularized native trabecular bovine bone. Solid tree line represents a statistically significant difference between time point of the same scaffold group; [a, b, c] represent statistically significant differences from 0% HA, 1.6% HA, and 3.1% HA, respectively, at the same time point.
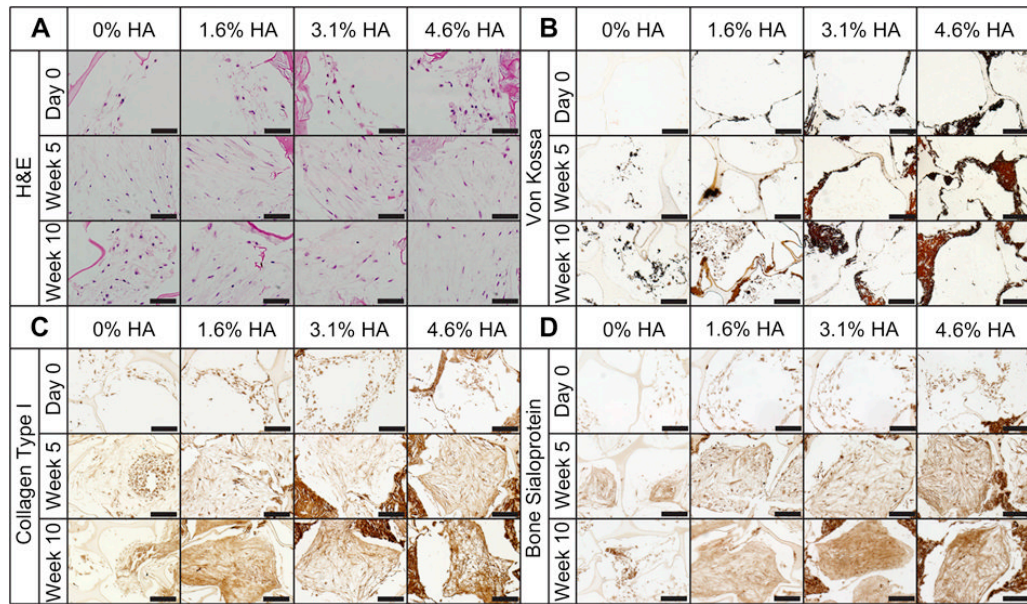
Figure 6.
Histology and immunohistochemistry of the constructs before and after cultivation: (A) H&E, (B) Von Kossa, (C) Collagen Type I, and (D) Bone sialoprotein (bar: 200 μm)
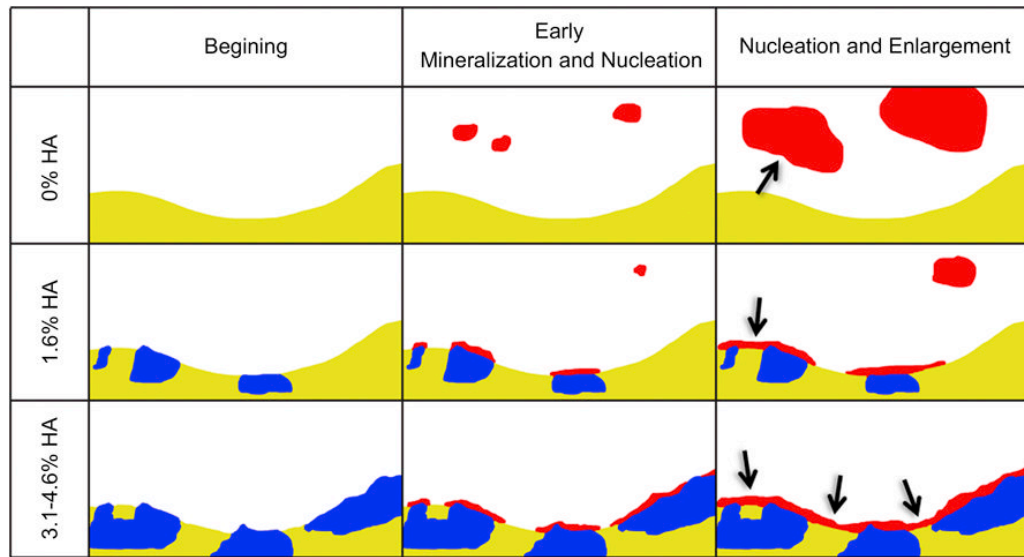
Figure 7.
Schematic of mineralization process. Yellow, blue and red regions represent silk, premineralized HA, and new mineral, respectively. Arrows indicate the connection of the new mineral structure. In 0% HA, newly produced mineral localized within the pore space and grew larger in size over time resulting in spherical-like mineral structure. In 1.6% HA, new mineral nucleated from premineralized HA as well as was deposited into the pore space. In 3.1-4.6% HA, the newly produced mineral nucleated from the premineralized HA. As the structure grew, structural connections occurred.